

# Properties of the one-dimensional Bose-Hubbard model from a high-order perturbative expansion

Bogdan Damski and Jakub Zakrzewski

*Instytut Fizyki imienia Mariana Smoluchowskiego,  
Uniwersytet Jagielloński, ulica Łojasiewicza 11, 30-348 Kraków, Poland*

We employ a high-order perturbative expansion to characterize the ground state of the Mott phase of the one-dimensional Bose-Hubbard model. We compute for different integer filling factors the energy per lattice site, the two-point and density-density correlations, and expectation values of powers of the on-site number operator determining the local atom number fluctuations (variance, skewness, kurtosis). We compare these expansions to numerical simulations of the infinite-size system to determine their range of applicability. We also discuss a new sum rule for the density-density correlations that can be used in both equilibrium and non-equilibrium systems.

## I. INTRODUCTION

The Bose-Hubbard models capture key properties of numerous experimentally-relevant configurations of cold bosonic atoms placed in optical lattices [1–4]. The simplest of them is defined by the Hamiltonian

$$\hat{H} = -J \sum_i \left( \hat{a}_{i+1}^\dagger \hat{a}_i + \text{h.c.} \right) + \frac{1}{2} \sum_i \hat{n}_i (\hat{n}_i - 1), \quad (1)$$

$$[\hat{a}_i, \hat{a}_j^\dagger] = \delta_{ij}, \quad [\hat{a}_i, \hat{a}_j] = 0, \quad \hat{n}_i = \hat{a}_i^\dagger \hat{a}_i,$$

where the first term describes tunnelling between adjacent sites, while the second one accounts for on-site interactions. The competition between these two terms leads to the Mott insulator–superfluid quantum phase transition when the filling factor (the mean number of atoms per lattice site) is integer [5, 6]. The system is in the superfluid phase when the tunnelling term dominates ( $J > J_c$ ) whereas it is in the Mott insulator phase when the interaction term wins out ( $J < J_c$ ). The location of the critical point depends on the filling factor  $n$  and the dimensionality of the system. We consider the one-dimensional model (1), where it was estimated that

$$J_c \approx \begin{cases} 0.3 & \text{for } n = 1 \\ 0.18 & \text{for } n = 2 \\ 0.12 & \text{for } n = 3 \end{cases}. \quad (2)$$

It should be mentioned that there is a few percent disagreement between different numerical computations of the position of the critical point (see Sec. 8.1 of Ref. [4] for an exhaustive discussion of this topic). That affects neither our results nor the discussion of our findings.

The Bose-Hubbard model (1), unlike some one-dimensional spin and cold atom systems [6, 7], is not exactly solvable. Therefore, it is not surprising that accurate analytical results describing its properties are scarce. To the best of our knowledge, the only systematic way of obtaining them is provided by the perturbative expansions [8–14]. In addition to delivering (free of finite-size effects) insights into physics of the Bose-Hubbard model, these expansions can be used to benchmark approximate approaches (see e.g. Refs. [15, 16]).

We compute the following ground-state expectation values: the energy per lattice site  $E$ , the two-point correlations  $C(r) = \langle \hat{a}_j^\dagger \hat{a}_{j+r} \rangle$ , the density-density correlations  $D(r) = \langle \hat{n}_j \hat{n}_{j+r} \rangle$ , and the powers of the on-site number operator  $Q(r) = \langle \hat{n}_i^r \rangle - n^r$ .

Our perturbative expansions are obtained with the technique described in Ref. [10] (see also Ref. [11] for a similar approach yielding the same results). The differences with respect to Ref. [10] are the following. First, we have computed perturbative expansions for the filling factors  $n = 2$  and  $3$ , which were not studied in Ref. [10]. Second, we have enlarged the order of all the expansions for the  $n = 1$  filling factor that were reported earlier. Moreover, several perturbative results for the  $n = 1$  case, that were not listed in Ref. [10], are provided in Appendix B. Third, we have computed perturbative expansions for the expectation values of different powers of the on-site atom number operator, which were not discussed in Ref. [10]. This allowed us for computation of the skewness and kurtosis characterizing on-site atom number distribution. Fourth, we have derived an important sum rule for the density-density correlations allowing for verification of all our perturbative expansions for these correlations.

The range of validity of our perturbative expansions is carefully established through numerical simulations. There is another crucial difference here with respect to our former work [10]. Namely, instead of considering a 40-site system, we study an infinite system using the translationally invariant version of the Time Evolving Block Decimation (TEBD)

algorithm sometimes referred to as iTEBD [17] (where i stands for infinite). The ground state of the system is found by imaginary time propagation [18]. For the detailed description of the method and its relation to the density matrix renormalization group studies see the excellent review [19]. The application of iTEBD allows for obtaining results free of the finite-size effects from numerical computations (see Appendix A for the details of these simulations). Our symbolic perturbative expansions have been done on a 256 Gb computer. The numerical computations require two orders of magnitude smaller computer memory.

The outline of this paper is the following. We discuss in Sec. II various identities that can be used to check the validity of our perturbative expansions. In particular, we derive there a sum rule for density-density correlation functions. Sec. III is focused on the ground state energy per lattice site. Sec. IV shows our results for the variance of the on-site atom number operator. Sec. V discusses expectation value of different powers of the on-site number operator and the related observables: the skewness and kurtosis of the local atom number distribution. Sec. VI discusses the two-point correlation functions. Sec. VII provides results on the density-density correlations. The perturbative expansions presented in Secs. III–VII are compared to numerics, which allows for establishing the range of their applicability. Additional perturbative expansions are listed in Appendices B, C, D for the filling factors  $n = 1, 2, 3$ , respectively. The paper ends with a brief summary (Sec. VIII).

## II. GROUND STATE IDENTITIES AND SUM RULE

There are several identities rigorously verifying our perturbative results. First, straight from the eigen-equation one gets that the ground state energy per lattice site,  $E$ , satisfies

$$E = -2JC(1) + \frac{D(0) - n}{2}. \quad (3)$$

It is easy to check that our perturbative expansions – (8), (12), and (27) for  $n = 1$ ; (9), (13), and (30) for  $n = 2$ ; and (10), (14), and (33) for  $n = 3$  – satisfy this identity.

Combining this result with the Feynman-Hellmann theorem,

$$\frac{d}{dJ}E = \left\langle \frac{d\hat{H}}{dJ} \right\rangle,$$

we get

$$\frac{d}{dJ}D(0) = 4J \frac{d}{dJ}C(1).$$

A similar identity can be found in Sec. 7.1 of Ref. [4]. Once again, it is straightforward to check that our expansions for  $n = 1, 2, 3$  satisfy this identity.

Finally, we obtain a sum rule for the density-density correlations in a one-dimensional system

$$D(0) - n^2 + 2 \sum_{r=1}^{\infty} [D(r) - n^2] = 0. \quad (4)$$

It is again an easy exercise to check that our expansions – (36)–(38) and (B6)–(B10) for  $n = 1$ ; (39)–(41) and (C5)–(C7) for  $n = 2$ ; and (42)–(44) and (D4)–(D6) for  $n = 3$  – satisfy this sum rule<sup>1</sup>. Eq. (4) can be obtained from the sum rule for the zeroth moment of the dynamic structure factor (see Ref. [20] for a general introduction to a dynamic structure factor and its sum rules and Ref. [21] for their discussion in a Bose-Hubbard model). We have, however, derived it in the following elementary way.

Consider a system of  $N$  atoms placed in the  $M$ -site periodic lattice ( $N, M < \infty$ ). Assuming that the system is prepared in an eigenstate of the number operator, say  $|\Psi\rangle$ , we have

$$N^2 = \left\langle \Psi \left| \left( \sum_{i=1}^M \hat{n}_i \right)^2 \right| \Psi \right\rangle = \sum_{i,j=1}^M \langle \Psi | \hat{n}_i \hat{n}_j | \Psi \rangle. \quad (5)$$

---

<sup>1</sup> There is no need to perform the sum over infinite number of  $D(r)$ 's to see that our results satisfy the sum rule (4). This follows from the observation that  $D(r > 0) - n^2 = O(J^{2r})$ . Thus, if our expansions for  $n = 1$  ( $n = 2$  and 3) are done up to the order  $J^{16}$  ( $J^{12}$ ), we need to know  $D(r)$  only for  $r = 1, 2, \dots, 8$  ( $r = 1, 2, \dots, 6$ ).

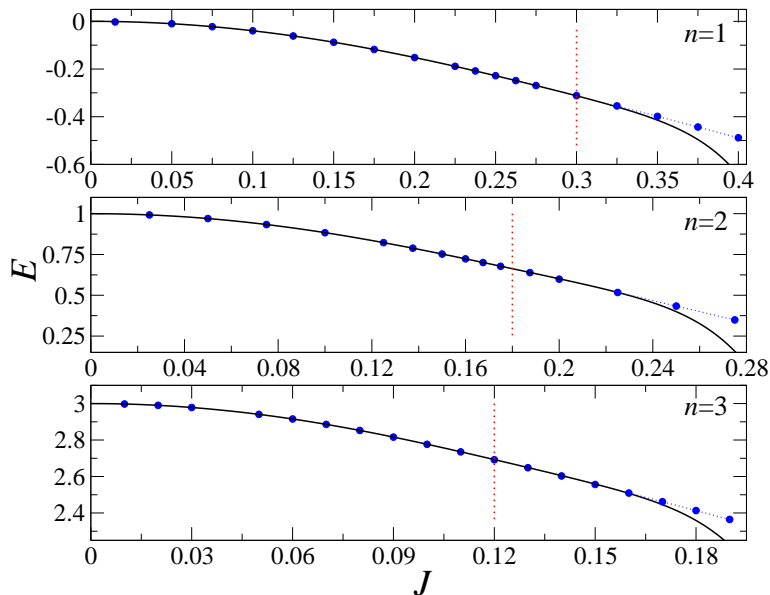


Figure 1: The energy per lattice site for different filling factors. Lines come from expansions (8)–(10), while dots show numerical results obtained using iTEBD code with the imaginary time evolution. Both here and in other figures we have (i) added blue dotted lines connecting the dots to facilitate quantification of the discrepancies between perturbative expansions and numerics; (ii) drawn red vertical dotted lines at the positions of the critical points; and (iii) used all the terms of the computed perturbative expansions listed in the paper to plot the perturbative results.

The next step is to assume that the correlations  $\langle \Psi | \hat{n}_i \hat{n}_j | \Psi \rangle$  depend only on the distance between the two lattice sites. This assumption allows for rewriting Eq. (5) to the form

$$D(0) - \left(\frac{N}{M}\right)^2 + 2 \sum_{r=1}^{\lfloor M/2 \rfloor} \left[ D(r) - \left(\frac{N}{M}\right)^2 \right] = 0, \quad (6)$$

where  $\lfloor x \rfloor$  stands for the largest integer not greater than  $x$ ,  $\lfloor M/2 \rfloor$  is the largest distance between two lattice sites in the  $M$ -site periodic lattice, and the prime in the sum indicates that in even-sized systems the summand for  $r = \lfloor M/2 \rfloor$  has to be multiplied by a factor  $1/2$ . One obtains Eq. (4) by taking the limit of  $N, M \rightarrow \infty$  such that the filling factor  $n = N/M$  is kept constant. Such a procedure is meaningful as long as the correlations  $D(r)$  tend to  $n^2$  sufficiently fast as  $r$  increases, which we assume. The extension of the above sum rule to two- and three-dimensional systems is straightforward, so we do not discuss it.

Instead, we mention that the sum rule (6) can be also applied to non-equilibrium systems satisfying the assumptions used in its derivation. It can be used either to study constraints on the dynamics of the density-density correlations or to verify the accuracy of numerical computations. Both applications are relevant for the studies of quench dynamics of the Bose-Hubbard model triggered by the time-variation of the tunnelling coupling  $J$  [22–24]. We mention in passing that a completely different work on the sum rules applicable to the Bose-Hubbard model can be found in Ref. [25].

Finally, we mention that it has been shown in Ref. [10] that the ground state energy per lattice site and the density-density correlations in the Bose-Hubbard model are unchanged by the

$$J \rightarrow -J \quad (7)$$

transformation, while the two-point correlations transform under (7) as  $C(r) \rightarrow (-1)^r C(r)$ . Using the same reasoning one can show that  $Q(r)$  is symmetric with respect to (7) as well. One can immediately check that all the expansions that we provide satisfy these rules. This observation provides one more consistency check of our perturbative expansions. Moreover, it allows us to skip the  $O(J^{m+2})$  term by the end of every expansion ending with a  $J^m$  term.

### III. GROUND STATE ENERGY

The ground state energy per lattice site  $E$  for the unit filling factor is

$$\begin{aligned} \frac{E}{4} = & -J^2 + J^4 + \frac{68}{9}J^6 - \frac{1267}{81}J^8 + \frac{44171}{1458}J^{10} - \frac{4902596}{6561}J^{12} - \frac{8020902135607}{2645395200}J^{14} \\ & - \frac{32507578587517774813}{466647713280000}J^{16}, \end{aligned} \quad (8)$$

while for  $n = 2$  it is given by

$$\begin{aligned} \frac{E}{4} = & \frac{1}{4} - 3J^2 + 8J^4 + \frac{49604}{315}J^6 - \frac{3385322797}{13891500}J^8 + \frac{8232891127289}{168469166250}J^{10} \\ & - \frac{7350064303936751836656911}{15282461406452625000}J^{12}, \end{aligned} \quad (9)$$

and finally for  $n = 3$  it reads

$$\begin{aligned} \frac{E}{4} = & \frac{3}{4} - 6J^2 + 31J^4 + \frac{73664}{63}J^6 - \frac{11207105017}{36117900}J^8 - \frac{76233225199535567419}{3516204203386875}J^{10} \\ & - \frac{39433892936615327274896871074109109}{1229047086250770739427475000}J^{12}. \end{aligned} \quad (10)$$

The ground state energy for an arbitrary integer filling factor was perturbatively calculated up to the  $J^4$  terms in Sec. 7.1 of Ref. [4]. Our expansions, of course, match this result.

A quick inspection of Fig. 1 reveals that there is an excellent agreement between numerics and finite-order perturbative expansions (8)–(10) not only in the whole Mott insulator phase, but also on the superfluid side near the critical point (see Ref. [16] for the same observation in the  $n = 1$  system). This is a bit surprising for two reasons.

First, it is expected that the perturbative expansions break down at the critical point in the thermodynamically-large systems undergoing a quantum phase transition. This, however, does not mean that our finite-order expansions (8)–(10) cannot accurately approximate ground state energy per lattice site across the critical point.

Second, we find it actually more surprising that despite the fact that our finite-order perturbative expansions for both  $C(1)$  and  $D(0)$  depart from the numerics on the Mott side, their combination (3) works so well across the critical point. The two-point correlation function  $C(1)$  is depicted in Figs. 8–10, while  $D(0)$  is given by  $\text{var}(\hat{n}) + n^2$ , where  $\text{var}(\hat{n})$  is plotted in Fig. 2. It would be good to understand whether this cancellation comes as a coincidence due to the finite-order of our perturbative expansions (8)–(10).

### IV. VARIANCE OF ON-SITE NUMBER OPERATOR

The most basic insight into the *local* fluctuations of the number of atoms in the ground state is delivered by the variance of the on-site number operator

$$\text{var}(\hat{n}) = \langle \hat{n}_i^2 \rangle - \langle \hat{n}_i \rangle^2 = D(0) - n^2. \quad (11)$$

This quantity is experimentally accessible due to the spectacular recent progress in the quantum gas microscopy [26].

We find that for the unit filling factor

$$\begin{aligned} \text{var}(\hat{n}) = & 8J^2 - 24J^4 - \frac{2720}{9}J^6 + \frac{70952}{81}J^8 - \frac{176684}{81}J^{10} + \frac{431428448}{6561}J^{12} + \frac{104271727762891}{330674400}J^{14} \\ & + \frac{32507578587517774813}{3888730944000}J^{16}, \end{aligned} \quad (12)$$

for the filling factor  $n = 2$

$$\begin{aligned} \text{var}(\hat{n}) = & 24J^2 - 192J^4 - \frac{396832}{63}J^6 + \frac{6770645594}{496125}J^8 - \frac{32931564509156}{9359398125}J^{10} \\ & + \frac{7350064303936751836656911}{173664334164234375}J^{12}, \end{aligned} \quad (13)$$

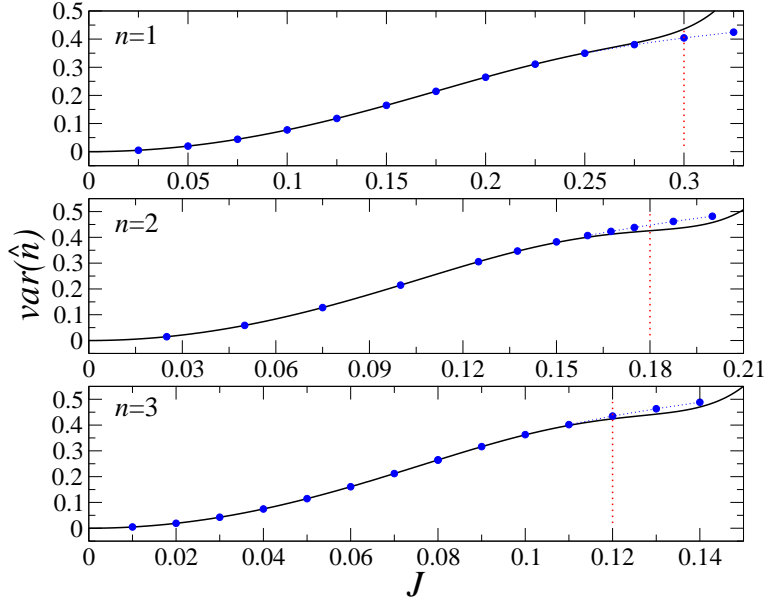


Figure 2: The variance (11) of the on-site atom number operator for the filling factors  $n = 1, 2, 3$ . Lines come from expansions (12)–(14), while the dots represent numerics.

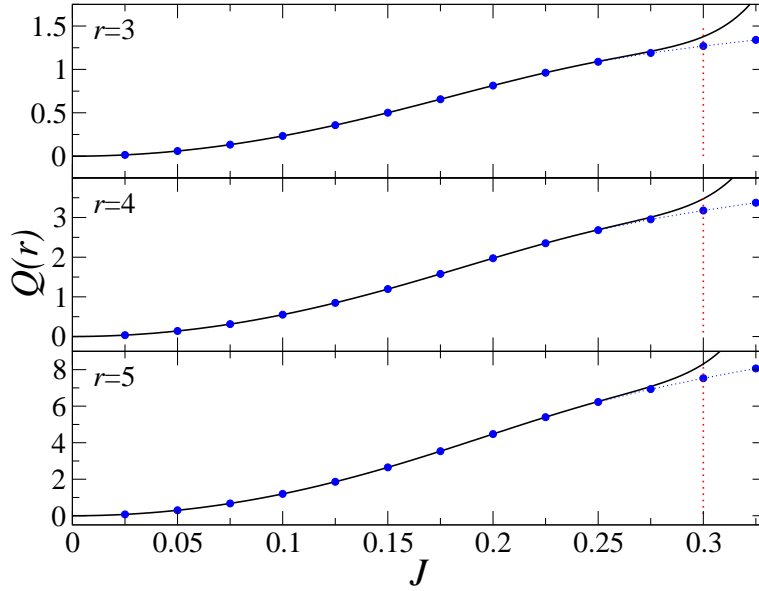


Figure 3: Expectation values of the powers of the on-site number operator (15) for the unit filling factor. Lines show expansions (16)–(18), while the dots show numerics.

and finally for  $n = 3$

$$\begin{aligned}
 \text{var}(\hat{n}) = & 48J^2 - 744J^4 - \frac{2946560}{63}J^6 + \frac{22414210034}{1289925}J^8 + \frac{609865801596284539352}{390689355931875}J^{10} \\
 & + \frac{39433892936615327274896871074109109}{13966444161940576584403125}J^{12}.
 \end{aligned} \tag{14}$$

The comparison between these perturbative expansions and numerics is presented in Fig. 2. We see there that our expansions accurately match numerics in most of the Mott phase and break down near the critical point. It might be worth to note that these on-site atom number fluctuations are nearly the same at the critical point (2) for the different filling factors (they equal roughly 0.4 there).

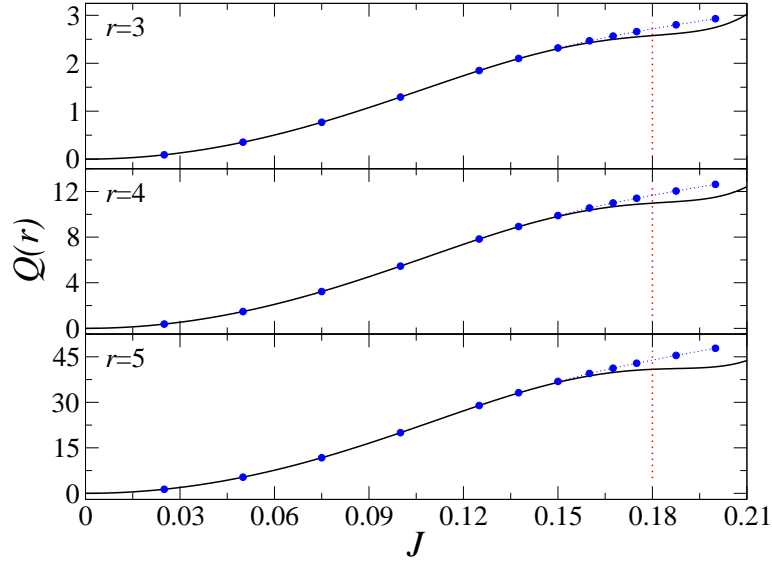


Figure 4: Expectation values of the powers of the on-site number operator (15) for the  $n = 2$  filling factor. Lines show expansions (19)–(21), while the dots show numerics.

## V. POWERS OF NUMBER OPERATOR

Further characterization of the fluctuations of the occupation of individual lattice sites comes from the study of expectation values of the integer powers of the on-site number operator

$$Q(r) = \langle \hat{n}_i^r \rangle - n^r \quad (15)$$

for  $r > 2$  (the  $r = 2$  case was analyzed in Sec. IV). Once again, we mention that these observables can be experimentally studied [26].

For the unit filling factor, we get

$$Q(3) = 24J^2 - 56J^4 - 976J^6 + \frac{185672}{81}J^8 - \frac{2584369}{243}J^{10} + \frac{11909666873}{52488}J^{12} + \frac{6518027091181469}{9258883200}J^{14} + \frac{5938172375134531873121}{181474110720000}J^{16}, \quad (16)$$

$$Q(4) = 56J^2 - 72J^4 - \frac{22784}{9}J^6 + \frac{355192}{81}J^8 - \frac{31533614}{729}J^{10} + \frac{16939285963}{26244}J^{12} + \frac{488931794121599}{661348800}J^{14} + \frac{12234501340429656667403}{116661928320000}J^{16}, \quad (17)$$

$$Q(5) = 120J^2 + 40J^4 - \frac{18800}{3}J^6 + \frac{601000}{81}J^8 - \frac{123485195}{729}J^{10} + \frac{31523026139}{17496}J^{12} - \frac{1978940191363981}{1322697600}J^{14} + \frac{2143214705361163325357}{6666395904000}J^{16}. \quad (18)$$

For two atoms per site, we obtain

$$Q(3) = 144J^2 - 1072J^4 - \frac{1913176}{49}J^6 + \frac{1770730207436}{24310125}J^8 - \frac{677140395560605171}{2162020966875}J^{10} + \frac{15451331550936239672643340032833}{60371453478515288484375}J^{12}, \quad (19)$$

$$Q(4) = 600J^2 - 3736J^4 - \frac{1885928848}{11025}J^6 + \frac{5417457952036}{40516875}J^8 - \frac{107844070676948560562}{32430314503125}J^{10} + \frac{59365618684278231437723679395069}{54883139525922989531250}J^{12}, \quad (20)$$

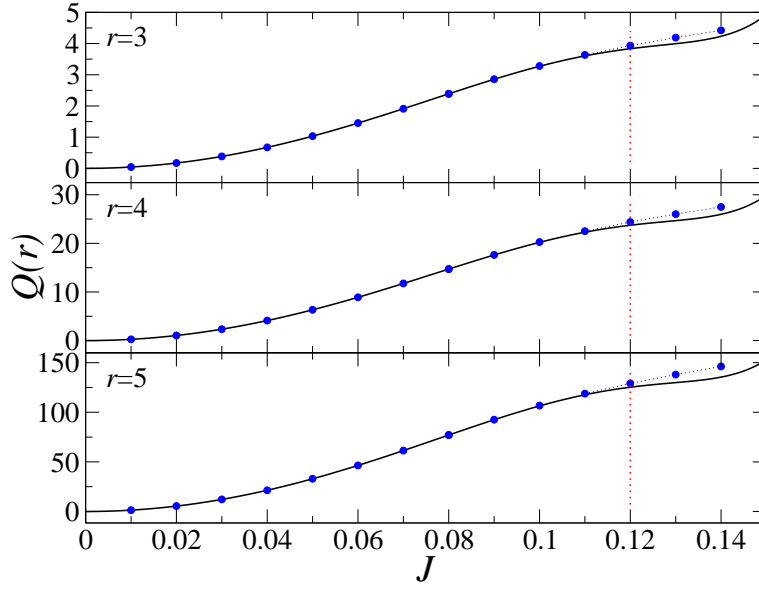


Figure 5: Expectation values of the powers of the on-site number operator (15) for the  $n = 3$  filling factor. Lines show expansions (22)–(24), while the dots show numerics.

$$Q(5) = 2160J^2 - 9440J^4 - \frac{483627832}{735}J^6 - \frac{12006980573744}{24310125}J^8 - \frac{52636963475404293323}{2162020966875}J^{10} + \frac{480125387136897585787036245853433}{120742906957030576968750}J^{12}. \quad (21)$$

Finally, for three atoms per site we derive

$$Q(3) = 432J^2 - 6472J^4 - \frac{1284712}{3}J^6 + \frac{1195336576618}{16769025}J^8 + \frac{27678339796268712326815412}{3184508940200713125}J^{10} + \frac{1273450413079818438111858514006273177409357}{50089814000150161485366743625000}J^{12}, \quad (22)$$

$$Q(4) = 2640J^2 - 36400J^4 - \frac{846750928}{315}J^6 - \frac{59064210154568}{23476635}J^8 - \frac{1031160890254623471701872}{974849675571646875}J^{10} + \frac{66279835521862060615675760372212019355789667}{425763419001276372625617320812500}J^{12}, \quad (23)$$

$$Q(5) = 13680J^2 - 163280J^4 - \frac{101064696}{7}J^6 - \frac{928759047058552}{23476635}J^8 - \frac{4229961332321756833865450804}{9553526820602139375}J^{10} + \frac{9189183527664354899691980380144063394455799}{11353691173367369936683128555000}J^{12}. \quad (24)$$

These expansions are compared to numerics in Figs. 3–5. They reproduce the numerics in the Mott insulator phase in the same range of the tunneling coupling  $J$  as our expansions for the variance of the on-site number operator.

Using expansions (16)–(24) one can easily go further, i.e., beyond the variance, in characterization of the on-site atom number distribution. For example, one can easily compute the skewness [27, 28]

$$S = \frac{\langle(\hat{n}_i - n)^3\rangle}{\langle(\hat{n}_i - n)^2\rangle^{3/2}} \quad (25)$$

and the kurtosis [27, 28] (also referred to as excess kurtosis)

$$K = \frac{\langle(\hat{n}_i - n)^4\rangle}{\langle(\hat{n}_i - n)^2\rangle^2} - 3. \quad (26)$$

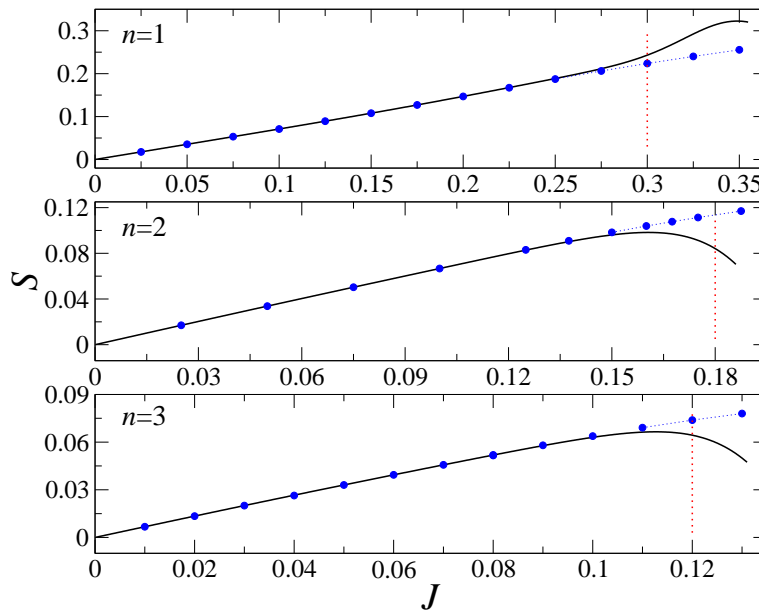


Figure 6: The skewness of the on-site atom number distribution. Lines show Eq. (25) computed with expansions from Secs. IV and V. Dots show numerics.

The skewness is a measure of a symmetry of the distribution. It is zero for a distribution that is symmetric around the mean. We plot the skewness in Fig. 6 and find it to be positive in the Mott insulator phase, which indicates that the distribution of different numbers of atoms is tilted towards larger-than-mean on-site occupation numbers. This is a somewhat expected result given the fact that the possible atom occupation numbers are bounded from below by zero and unbounded from above. Given the fact that  $|S| < 1/2$  in Fig. 6, one may conclude that the on-site atom number distribution is “fairly symmetric” in the Mott phase according to the criteria from Ref. [28].

The kurtosis quantifies whether the distribution is peaked or flat relative to the normal (Gaussian) distribution. It is calibrated such that it equals zero for the normal distribution of arbitrary mean and variance.  $K > 0$  ( $K < 0$ ) indicates that the studied distribution is peaked (flattened) relative to the normal distribution. We plot the kurtosis in Fig. 7. As  $J \rightarrow 0$  one easily finds from our expansions that  $K \sim J^{-2}$ . This singularity reflects the strong suppression of the local atom number fluctuations in the deep Mott insulator limit. The kurtosis monotonically decays in the Mott phase (Fig. 7).

To put these results in context, we compare them to the on-site atom number distribution in the deep superfluid limit of  $J \rightarrow \infty$  (the Poisson distribution [29]). The probability of finding  $s$  atoms in a lattice site is then given in the thermodynamic limit by  $\exp(-n)n^s/s!$ , where  $n$  is the mean occupation. One then finds that  $S = 1/\sqrt{n}$  and  $K = 1/n$  for the Poisson distribution. Keeping in mind that the Gaussian distribution is characterized by  $S = K = 0$ , we can try to see whether the on-site atom number distribution near the critical point is Gaussian-like or Poissonian-like.

We see from Figs. 6 and 7 that at the critical point (2) we have  $S \approx 0.22, 0.11, 0.07$  and  $K \approx 0.19, 0.3, 0.4$  for  $n = 1, 2, 3$ , respectively. Therefore, the real distribution lies somehow between Poissonian and Gaussian. The skewness suggests that for these filling factors the distribution at the critical point is more Gaussian than Poissonian. On the other hand, the kurtosis for  $n = 1$  ( $n = 2, 3$ ) is more Gaussian (Poissonian). From this we conclude that for the unit filling factor the on-site atom number distribution at the critical point is better approximated by the Gaussian distribution.

## VI. TWO-POINT CORRELATIONS

The two-point correlation functions play a special role in the cold atom realizations of the Bose-Hubbard model [30–32]. Their Fourier transform provides the quasi-momentum distribution of a cold atom cloud, which is visible through the time-of-flight images that are taken after releasing the cloud from the trap.



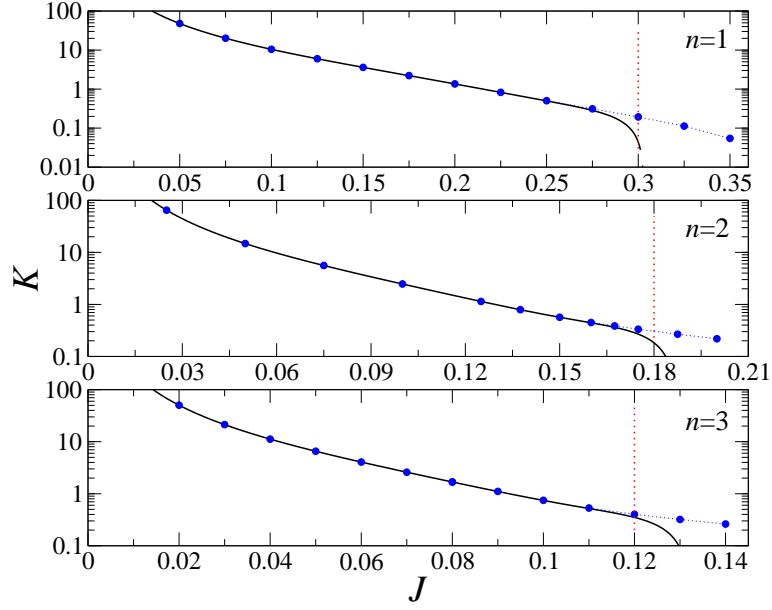


Figure 7: The kurtosis of the on-site atom number distribution. Lines show Eq. (26) computed with expansions from Secs. IV and V. Dots show numerics.

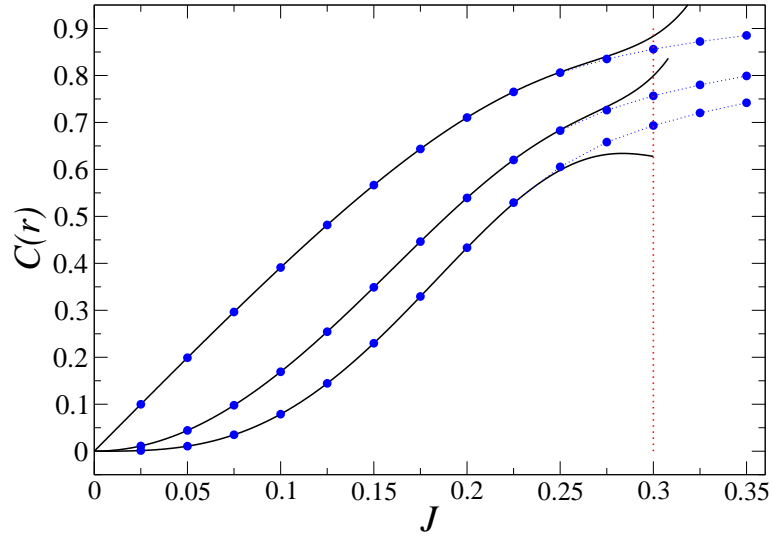


Figure 8: The two-point correlation functions for the unit filling factor. Lines from top to bottom correspond to  $r = 1, 2, 3$ , respectively. They depict perturbative expansions (27)–(29). The numerics is presented with dots.

For the filling factor  $n = 1$ , they are given by

$$C(1) = 4J - 8J^3 - \frac{272}{3}J^5 + \frac{20272}{81}J^7 - \frac{441710}{729}J^9 + \frac{39220768}{2187}J^{11} + \frac{8020902135607}{94478400}J^{13} + \frac{32507578587517774813}{14582741040000}J^{15}, \quad (27)$$

$$C(2) = 18J^2 - \frac{320}{3}J^4 - \frac{1826}{9}J^6 + \frac{234862}{243}J^8 + \frac{345809}{2916}J^{10} + \frac{4434868108963}{220449600}J^{12} + \frac{94620702880069301837}{38887309440000}J^{14}, \quad (28)$$

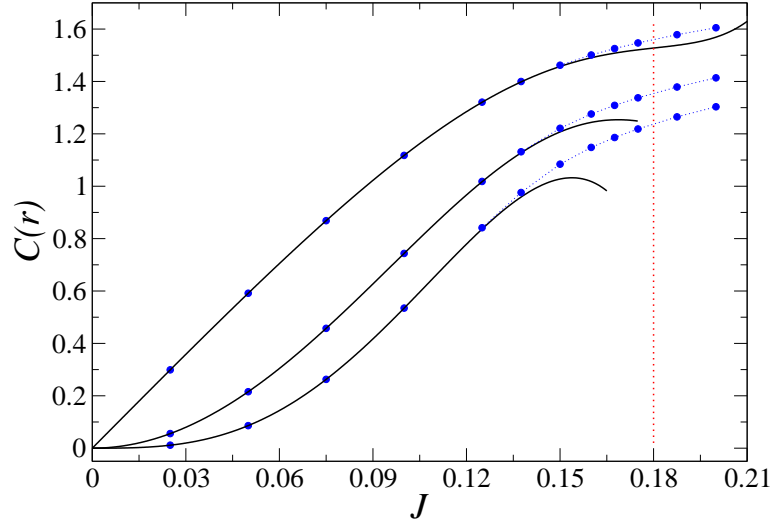


Figure 9: The two-point correlation functions for the  $n = 2$  filling factor. Lines from top to bottom correspond to  $r = 1, 2, 3$ , respectively. They depict perturbative expansions (30)–(32). The numerics is presented with dots.

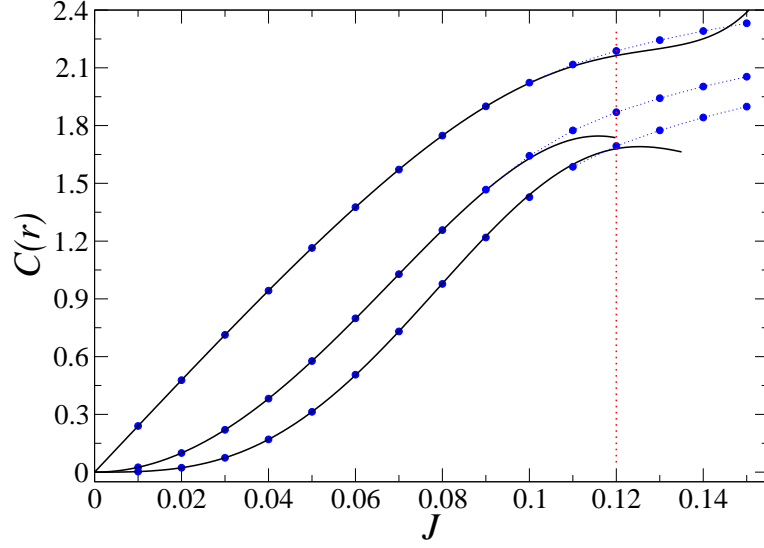


Figure 10: The two-point correlation functions for the  $n = 3$  filling factor. Lines from top to bottom correspond to  $r = 1, 2, 3$ , respectively. They depict perturbative expansions (33)–(35). The numerics is presented with dots.

$$\begin{aligned}
 C(3) = & 88J^3 - \frac{8324}{9}J^5 + \frac{126040}{81}J^7 + \frac{7883333}{486}J^9 - \frac{220980576341}{1049760}J^{11} \\
 & + \frac{82283484127688477}{61725888000}J^{13},
 \end{aligned} \tag{29}$$

and for the filling factor  $n = 2$  they are

$$\begin{aligned}
 C(1) = & 12J - 64J^3 - \frac{198416}{105}J^5 + \frac{13541291188}{3472875}J^7 - \frac{16465782254578}{16846916625}J^9 \\
 & + \frac{7350064303936751836656911}{636769225268859375}J^{11},
 \end{aligned} \tag{30}$$

$$\begin{aligned}
 C(2) = & 90J^2 - \frac{4520}{3}J^4 - \frac{12971657}{2205}J^6 - \frac{290416211186}{16372125}J^8 + \frac{15957686927590379575531}{10511745940946250}J^{10} \\
 & + \frac{651222142925783091305873230764520129}{10926355845430110013929000000}J^{12},
 \end{aligned} \tag{31}$$

$$C(3) = 744J^3 - \frac{201172}{9}J^5 + \frac{467115289252}{3472875}J^7 + \frac{934116436332193243}{617720276250}J^9 - \frac{165376430398934085307383814830617}{1931886511312489231500000}J^{11}, \quad (32)$$

and finally for  $n = 3$  they read

$$C(1) = 24J - 248J^3 - \frac{294656}{21}J^5 + \frac{44828420068}{9029475}J^7 + \frac{304932900798142269676}{703240840677375}J^9 + \frac{39433892936615327274896871074109109}{51210295260448780809478125}J^{11}, \quad (33)$$

$$C(2) = 252J^2 - \frac{24920}{3}J^4 - \frac{2559347}{45}J^6 - \frac{912812009912144}{774728955}J^8 + \frac{728914146234298491592146132346}{8932547577263000315625}J^{10}, \quad (34)$$

$$C(3) = 2928J^3 - \frac{1563584}{9}J^5 + \frac{60570509140}{27783}J^7 + \frac{21318637245947810350682}{678565723460625}J^9. \quad (35)$$

Expansions up to the order  $J^3$  for  $C(1)$ ,  $C(2)$ , and  $C(3)$  at arbitrary integer filling factors are listed in Sec. 7.1 of Ref. [4] and agree with our results.

We see in Figs. 8–10 that the above perturbative expansions break down within the Mott insulator phase (the larger  $r$ , the deeper in the Mott phase the expansion breaks down). We notice that it is instructive to compare the value of the correlations  $C(r)$  around the critical point to their deep superfluid limit.  $C(r)$  in the  $J \rightarrow \infty$  limit tends to  $n$  (see e.g. Appendix B of Ref. [10]). Therefore, the three correlation functions  $C(r = 1, 2, 3)$  reach at least 50% of their deep superfluid value near the critical point, which well illustrates the significance of quantum fluctuations at the critical point.

The ground state quasi-momentum distribution is defined as

$$\tilde{n}(k) = \frac{1}{M} \sum_{m,s=1}^M \langle \hat{a}_m^\dagger \hat{a}_s \rangle \exp[ik(m-s)],$$

where  $M$  stands for the number of lattice sites (we skip the prefactor proportional to the squared modulus of the Fourier transform of the Wannier functions; see Ref. [31] for details). Taking the limit of  $M \rightarrow \infty$  at the fixed integer filling factor  $n$ , one gets

$$\tilde{n}(k) = n + 2 \sum_{r=1}^{\infty} C(r) \cos(rk).$$

Using Eqs. (27)–(29) and (B1)–(B5) for  $n = 1$ , Eqs. (30)–(32) and (C1)–(C4) for  $n = 2$ , and Eqs. (33)–(35) and (D1)–(D3) for  $n = 3$  the state-of-the-art high-order perturbative quasi-momentum distributions for different filling factors can be obtained. These results can be compared to Ref. [14], where an expression with terms up to  $J^3$  for an arbitrary filling factor is computed. As expected, we find these results in agreement with our findings.

## VII. DENSITY-DENSITY CORRELATIONS

Similarly as the observables from Secs. IV and V, the density-density correlations can be experimentally approached through the technique discussed in Ref. [26].

The density-density correlations are given for  $n = 1$  by

$$D(1) = 1 - 4J^2 + \frac{136}{3}J^4 - \frac{2008}{27}J^6 - \frac{150638}{81}J^8 + \frac{4897282}{729}J^{10} - \frac{415922848153}{14696640}J^{12} + \frac{1022120948444278027}{7777461888000}J^{14} + \frac{4588274318283441920855291}{2515231174579200000}J^{16}, \quad (36)$$

$$D(2) = 1 - \frac{100}{3}J^4 + \frac{2128}{3}J^6 - \frac{1156462}{243}J^8 - \frac{6848011}{729}J^{10} + \frac{10808763042127}{44089920}J^{12} - \frac{5150051155340205251}{3888730944000}J^{14} - \frac{10173100607048978123860781}{15091387047475200000}J^{16}, \quad (37)$$

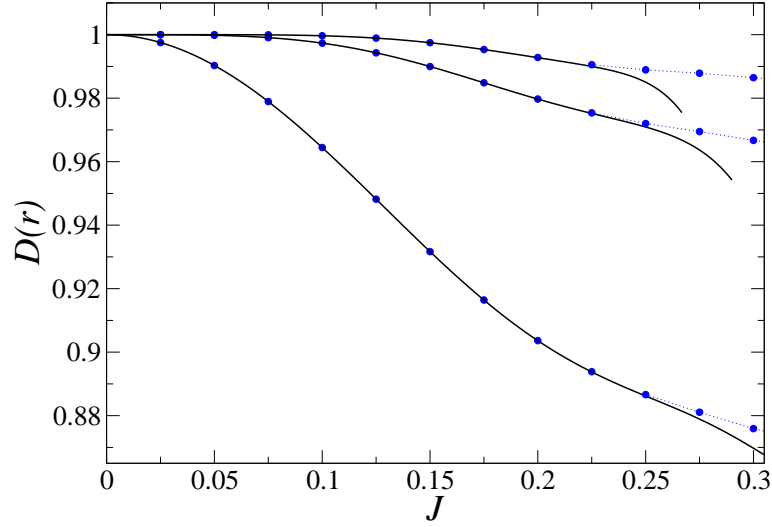


Figure 11: The density-density correlation functions for the unit filling factor. Lines from bottom to top illustrate perturbative results for  $r = 1, 2, 3$ , respectively. Dots show numerics. Perturbative expansions are given by Eqs. (36)–(38).

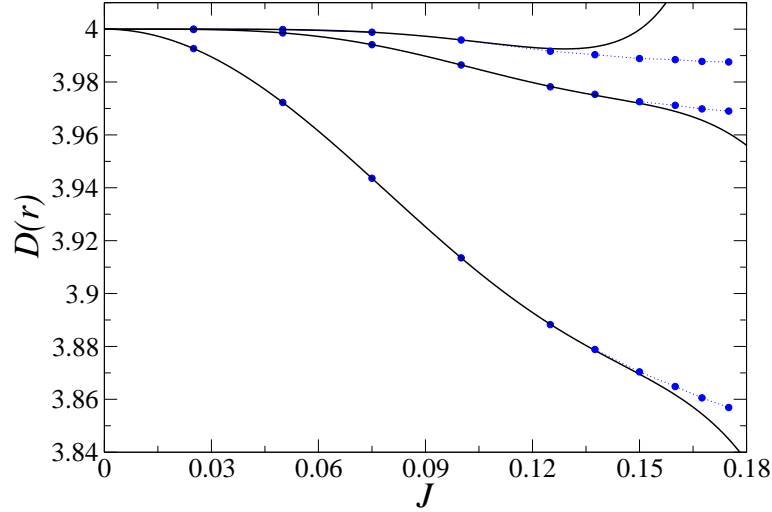


Figure 12: The density-density correlation functions for the  $n = 2$  filling factor. Lines from bottom to top illustrate perturbative results for  $r = 1, 2, 3$ , respectively. Dots show numerics. Perturbative expansions are given by Eqs. (39)–(41).

$$\begin{aligned}
 D(3) = & 1 - \frac{13064}{27}J^6 + \frac{3727066}{243}J^8 - \frac{1588041877}{8748}J^{10} + \frac{1710030328933}{2755620}J^{12} \\
 & + \frac{2208787916976404357}{370355328000}J^{14} - \frac{73297040097456632572895911}{1006092469831680000}J^{16},
 \end{aligned} \tag{38}$$

for  $n = 2$  they read

$$\begin{aligned}
 D(1) = & 4 - 12J^2 + \frac{1100}{3}J^4 - \frac{80553632}{33075}J^6 - \frac{8915569805768}{121550625}J^8 - \frac{185683648947492811}{6486062900625}J^{10} \\
 & + \frac{331686439652436848222471319678887}{72445744174218346181250000}J^{12},
 \end{aligned} \tag{39}$$

$$\begin{aligned}
 D(2) = & 4 - \frac{812}{3}J^4 + \frac{189419192}{11025}J^6 - \frac{140772979852859}{364651875}J^8 + \frac{569733162420769673609}{324303145031250}J^{10} \\
 & + \frac{8056033392249986400009146407648}{503095445654294070703125}J^{12},
 \end{aligned} \tag{40}$$

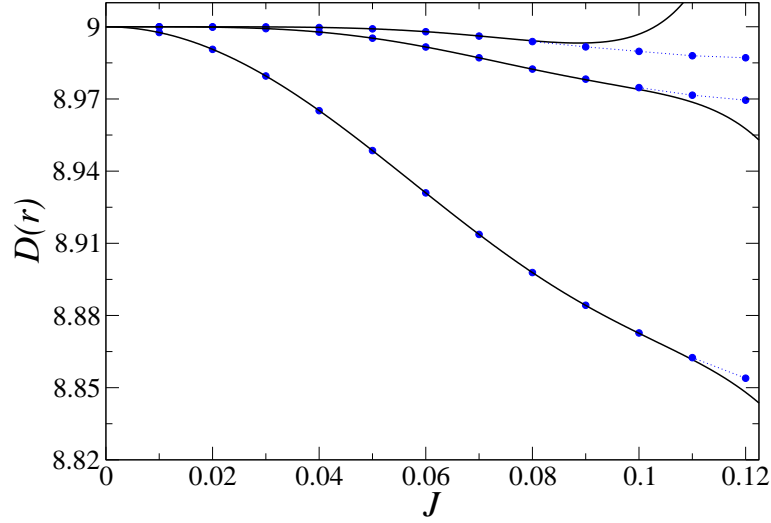


Figure 13: The density-density correlation functions for the  $n = 3$  filling factor. Lines from bottom to top illustrate perturbative results for  $r = 1, 2, 3$ , respectively. Dots show numerics. Perturbative expansions are given by Eqs. (42)–(44).

$$D(3) = 4 - \frac{7827256}{675}J^6 + \frac{79648906064158}{72930375}J^8 - \frac{79481781249654943885127}{1945818870187500}J^{10} + \frac{1369141430325035192671991031520835051}{2028480836878113693075000000}J^{12}. \quad (41)$$

and finally for  $n = 3$  they can be written as

$$D(1) = 9 - 24J^2 + \frac{4276}{3}J^4 - \frac{134562824}{6615}J^6 - \frac{3678796866393562}{4108411125}J^8 - \frac{2257554577848066943151996417}{200624063232644926875}J^{10} + \frac{1542480719505910230376228320731168033769541}{3193225642509572794692129906093750}J^{12}, \quad (42)$$

$$D(2) = 9 - \frac{3160}{3}J^4 + \frac{294843464}{2205}J^6 - \frac{76035818562996449}{12325233375}J^8 + \frac{83670951564711862884744588592}{1003120316163224634375}J^{10} - \frac{143706393091669463828236051561683582721397}{132705481247151077182010593500000}J^{12}, \quad (43)$$

$$D(3) = 9 - \frac{12148432}{135}J^6 + \frac{246576902129764}{14586075}J^8 - \frac{1185488040768577918685665169}{926242212523753125}J^{10} + \frac{13080624640958701853202057691706510935349239}{285200376364491350084145573750000}J^{12}. \quad (44)$$

The correlation functions  $D(1)$  and  $D(2)$  were computed for an arbitrary integer filling factor up to the order  $J^4$  in Sec. 7.1 of Ref. [4]. These results agree with our expansions.

The comparison between our perturbative expansions and numerics is presented in Figs. 11–13 for different filling factors. The expansions break down near the critical point on the Mott side of the transition. Comparing Figs. 8–10 to Figs. 11–13, we see that expansions for the two-point and density-density correlations break down in similar distances from the critical point. Moreover, this comparison shows that the two-point correlations change more appreciably within the Mott phase than the density-density correlations. We attribute it to the constraints that are imposed on the density-density correlations due to the atom number conservation.

## VIII. SUMMARY

We have computed state-of-the-art high-order perturbative expansions for several observables characterizing ground state properties of the one-dimensional Bose-Hubbard model in the Mott phase. As compared to our former results

for the filling factor  $n = 1$  [10], we have extended our analysis by considering the filling factors  $n = 2$  and  $3$  (we have also enlarged the number of terms for the  $n = 1$  case). We have characterized the on-site atom number distribution by giving the predictions for the skewness and kurtosis. Those may serve as useful benchmarks for experimental in-situ observations [26]. We have also derived in a simple way an important sum rule applicable to both equilibrium and non-equilibrium density-density correlations. That sum rule allows for verification of our perturbative expansions and it may be useful for checking the consistency of experimental data. We have also carefully established the range of applicability of our perturbative expansions through numerical simulations. The expansions discussed in this work can be easily typed or imported into computer software such as **Mathematica** or **Maple** and used for benchmarking approximate approaches, comparing theoretical predictions to experimental measurements, testing Padé approximations, etc.

## IX. ACKNOWLEDGMENT

BD thanks Eddy Timmermans for a discussion about sum rules that happened about a decade ago. JZ acknowledges the collaboration with Dominique Delande on developing the implementation of the iTEBD code. We acknowledge support of Polish National Science Centre via projects DEC-2013/09/B/ST3/00239 (BD) and DEC-2012/04/A/ST2/00088 (JZ). Support from the EU Horizon 2020-FET QUIC 641122 is also acknowledged (JZ).

## Appendix A: iTEBD simulations

There are two factors that have to be taken care of to assure the convergence of results in the numerical implementation of iTEBD. The first one is the maximal allowed number of bosons per site assumed in the variational ansatz,  $N_{max}$ . We take  $N_{max} = 6$  for the filling factor  $n = 1$  up to  $N_{max} = 12$  for  $n = 3$ . We have checked that these values lead to converged results. The second important factor is the number of Schmidt decomposition eigenvalues,  $\chi$ , kept during each step of the procedure [17, 19].  $\chi$  may be quite small deep in the Mott regime (of about 20) while it must be significantly increased close to the critical point and in the superfluid regime. We have found that for reliable energy, particle number variance, as well as two-point correlations with small  $r$  the choice of  $\chi = 150$  was largely enough (with the relative error of the order of  $10^{-7}$  in energy and  $10^{-5}$  in particle number variance). Let us note that the numerical studies of long-range correlations ( $r$  of the order of a hundred) require taking  $\chi > r$  at least [18].

## Appendix B: One atom per site

Our remaining perturbative expansions for the  $n = 1$  filling factor are listed below.  
The two-point correlations:

$$C(4) = 450J^4 - \frac{186608}{27}J^6 + \frac{7565704}{243}J^8 + \frac{1493509507}{17496}J^{10} - \frac{858313783040137}{440899200}J^{12}, \quad (B1)$$

$$C(5) = 2364J^5 - \frac{3894512}{81}J^7 + \frac{250517014}{729}J^9 - \frac{25842700043}{209952}J^{11}, \quad (B2)$$

$$C(6) = 12642J^6 - \frac{78008768}{243}J^8 + \frac{6836492080}{2187}J^{10}, \quad (B3)$$

$$C(7) = 68464J^7 - \frac{1522020908}{729}J^9, \quad (B4)$$

$$C(8) = 374274J^8. \quad (B5)$$

The density-density correlations:

$$\begin{aligned} D(4) = & 1 - \frac{741706}{81}J^8 + \frac{93328235}{243}J^{10} - \frac{288653212433561}{44089920}J^{12} + \frac{32675495835088308133}{648121824000}J^{14} \\ & - \frac{136868524145553747592735387}{5030462349158400000}J^{16}, \end{aligned} \quad (B6)$$

$$D(5) = 1 - \frac{1738824899}{8748}J^{10} + \frac{91423339623697}{8817984}J^{12} - \frac{897923823504590743589}{3888730944000}J^{14} + \frac{40404128939318210395355039327}{15091387047475200000}J^{16}, \quad (B7)$$

$$D(6) = 1 - \frac{369347437555}{78732}J^{12} + \frac{22768945554355275259}{77774618880}J^{14} - \frac{20246612891148030348297322711}{2515231174579200000}J^{16}, \quad (B8)$$

$$D(7) = 1 - \frac{1771595060952703}{15116544}J^{14} + \frac{4869453765809764188858679}{571643448768000}J^{16}, \quad (B9)$$

$$D(8) = 1 - \frac{415126490285461535}{136048896}J^{16}. \quad (B10)$$

### Appendix C: Two atoms per site

Our remaining perturbative expansions for the  $n = 2$  filling factor are listed below.  
The two-point correlations:

$$C(4) = 6450J^4 - \frac{7683200}{27}J^6 + \frac{291093977979158}{72930375}J^8 + \frac{10163319115920107956583}{1712320605765000}J^{10}, \quad (C1)$$

$$C(5) = 57492J^5 - \frac{272806072}{81}J^7 + \frac{2786470218115003978}{38288446875}J^9, \quad (C2)$$

$$C(6) = 521850J^6 - \frac{9291088760}{243}J^8, \quad (C3)$$

$$C(7) = 4797840J^7. \quad (C4)$$

The density-density correlations:

$$D(4) = 4 - \frac{1586483355826}{2480625}J^8 + \frac{25731787904762281349459}{324303145031250}J^{10} - \frac{4867179143263377024841830332580901}{1169827472248047112500000}J^{12}, \quad (C5)$$

$$D(5) = 4 - \frac{13200913614880820989}{328186687500}J^{10} + \frac{43439587507699792960803904702410359}{7018964833488282675000000}J^{12}, \quad (C6)$$

$$D(6) = 4 - \frac{231224301660078686005531}{84234583125000}J^{12}. \quad (C7)$$

### Appendix D: Three atoms per site

Our remaining perturbative expansions for the  $n = 3$  filling factor are listed below.  
The two-point correlations:

$$C(4) = 35700J^4 - \frac{84091952}{27}J^6 + \frac{919114524688124}{10418625}J^8, \quad (D1)$$

$$C(5) = 447624J^5 - \frac{4203103112}{81}J^7, \quad (D2)$$

$$C(6) = 5715948J^6. \quad (D3)$$

The density-density correlations:

$$D(4) = 9 - \frac{977276150432}{99225} J^8 + \frac{21533082002709807426464}{8844631228125} J^{10} - \frac{13390761501371812933197864158162939174976229}{52141897063868224669123567500000} J^{12}, \quad (D4)$$

$$D(5) = 9 - \frac{20144790858435740956}{16409334375} J^{10} + \frac{74244526197167849189627032046547619}{197408385941857950234375} J^{12}, \quad (D5)$$

$$D(6) = 9 - \frac{242194363655594937438210358}{1459364152640625} J^{12}. \quad (D6)$$

- 
- [1] D. Jaksch and P. Zoller, Ann. Phys. **315**, 52 (2005).
  - [2] M. Lewenstein, A. Sanpera, and V. Ahufinger, *Ultracold Atoms in Optical Lattices: Simulating Quantum Many-Body Systems* (Oxford University Press, Oxford, UK, 2012).
  - [3] O. Dutta, M. Gajda, P. Hauke, M. Lewenstein, D.-S. Lühmann, B.A. Malomed, T. Sowiński, and J. Zakrzewski, Rep. Prog. Phys. **78**, 066001 (2015).
  - [4] K.V. Krutitsky, *e-print* arXiv:1501.03125.
  - [5] M. P. A. Fisher, P. B. Weichman, G. Grinstein, and D. S. Fisher, Phys. Rev. B **40**, 546 (1989).
  - [6] S. Sachdev, *Quantum Phase Transitions* (Cambridge University Press, 2011).
  - [7] M. Gaudin, *The Bethe Wavefunction* (Cambridge University Press, 2014).
  - [8] J. K. Freericks and H. Monien, Phys. Rev. B **53**, 2691 (1996).
  - [9] N. Elstner and H. Monien, Phys. Rev. B **59**, 12184 (1999); *e-print* arXiv:cond-mat/9905367 (unpublished).
  - [10] B. Damski and J. Zakrzewski, Phys. Rev. A **74**, 043609 (2006).
  - [11] N. Teichmann, D. Hinrichs, M. Holthaus, and A. Eckardt, Phys. Rev. B **79**, 224515 (2009).
  - [12] A. Eckardt, Phys. Rev. B **79**, 195131 (2009).
  - [13] S. Sanders, C. Heinisch, and M. Holthaus, Europhys. Lett. **111**, 20002 (2015).
  - [14] J. K. Freericks, H. R. Krishnamurthy, Y. Kato, N. Kawashima, and N. Trivedi, Phys. Rev. A **79**, 053631 (2009).
  - [15] M. Knap, E. Arrigoni, and W. von der Linden, Phys. Rev. B **81**, 235122 (2010).
  - [16] S. Ejima, H. Fehske, F. Gebhard, K. zu Münster, M. Knap, E. Arrigoni, and W. von der Linden, Phys. Rev. A **85**, 053644 (2012).
  - [17] G. Vidal, Phys. Rev. Lett. **98**, 070201 (2007).
  - [18] J. Zakrzewski and D. Delande, in *Proceedings of Let's Face Chaos Through Nonlinear Dynamics, 7th International Summer School and Conference*, Vol. 1076 (AIP, Melville, NY, 2008), pp. 292–300.
  - [19] U. Schollwöck, Ann. Phys. (NY) **326**, 96 (2011).
  - [20] L. Pitaevskii and S. Stringari, *Bose–Einstein Condensation* (Clarendon Press, 2003).
  - [21] R. Roth and K. Burnett, J. Phys. B **37**, 3893 (2004).
  - [22] A.M. Läuchli and C. Kollath, J. Stat. Mech. (2008) P05018.
  - [23] P. Barmettler, D. Poletti, M. Cheneau, and C. Kollath, Phys. Rev. A **85**, 053625 (2012).
  - [24] G. Carleo, F. Becca, L. Sanchez-Palencia, S. Sorella, and M. Fabrizio, Phys. Rev. A **89**, 031602 (2014).
  - [25] J. K. Freericks, V. Turkowski, H. R. Krishnamurthy, and M. Knap, Phys. Rev. A **87**, 013628 (2013).
  - [26] P. M. Preiss, R. Ma, M. E. Tai, J. Simon, and M. Greiner, Phys. Rev. A **91**, 041602 (2015).
  - [27] NIST/SEMATECH e-Handbook of Statistical Methods, <http://www.itl.nist.gov/div898/handbook/>.
  - [28] M.G. Bulmer, *Principles of Statistics* (Dover, New York, 1979).
  - [29] B. Capogrosso-Sansone, E. Kozik, N. Prokof'ev, and B. Svistunov, Phys. Rev. A **75**, 013619 (2007).
  - [30] M. Greiner, O. Mandel, T. Esslinger, T. W. Hänsch, and I. Bloch, Nature (London) **415**, 39 (2002).
  - [31] V. A. Kashurnikov, N. V. Prokof'ev, and B. V. Svistunov, Phys. Rev. A **66**, 031601 (2002).
  - [32] I. Bloch, J. Dalibard, and W. Zwerger, Rev. Mod. Phys. **80**, 885 (2008).